Research Article

Maha Abdallah Alnuwaiser, Mohamed Rabia*, and Asmaa M. Elsayed*

Bismuthyl chloride/poly(*m*-toluidine) nanocomposite seeded on poly-1*H* pyrrole: Photocathode for green hydrogen generation

https://doi.org/10.1515/phys-2024-0111
received October 30, 2024; accepted December 25, 2024

Abstract: A novel photocathode has been developed for H_2 gas generation from sewage water, utilizing a bismuthyl chloride–poly *m*-toluidine (BiOCl–PMT) nanocomposite supported on poly-1*H* pyrrole (P1HP). X-Ray photoelectron spectroscopy analysis confirms the formation of bismuth oxide intercalated within the polymer network through a chemical reaction, resulting in the creation of bismuth oxide chloride (BiOCl). This photocathode exhibits strong absorption in the UV region, extending into the visible spectrum, with a bandgap of 2.75 eV, enabling effective interaction with photons and efficient energy transfer to the photocatalyst nanomaterials. The material's crystalline size is limited to 39 nm, and it features a highly porous polymer structure with a pore size of 20 nm, aggregating into larger structures approximately 300 nm thick. When employed as the working electrode in a three-electrode cell, the BiOCl/PMT/P1HP photocathode shows a measured photocurrent density (J_{ph}) of −0.046 mA/cm² under illumination, which drops to −0.032 mA/cm² when the light is turned off. The resulting photocurrent of 0.012 mA/cm² reflects the photocathode's efficient photoelectrochemical behavior. The performance of the photocathode during sewage water splitting can be adjusted by varying the photon energies between 3.6 and 1.7 eV, using filters to control photon wavelengths. This variation is evident in the linear sweep voltammetry curves, with J_{ph} values ranging from −0.045 mA/cm² at 3.4 eV to about −0.042 mA/cm² at 1.7 eV under an applied bias voltage of −0.7 V. The photocathode's high efficiency is further demonstrated by its ability to produce 15 μmol/h of H_2 gas for a 10 cm² area. This promising performance, combined with cost-effectiveness, makes the BiOCl/PMT/P1HP photocathode an attractive option for green chemistry and industrial applications.

Keywords: bismuthyl chloride, poly(*m*-toluidine), nanocomposite, photocathode, hydrogen generation

*** Corresponding author: Mohamed Rabia,** Nanomaterials Science Research Laboratory, Chemistry Department, Faculty of Science, Beni-Suef University, Beni-Suef, 62514, Egypt,
e-mail: mohamedchem@science.bsu.edu.eg
*** Corresponding author: Asmaa M. Elsayed,** TH-PPM Group, Physics Department, Faculty of Science, Beni-Suef University, Beni-Suef, 62514, Egypt, e-mail: Asmaa.elsayed@science.bsu.edu.eg
Maha Abdallah Alnuwaiser: Department of Chemistry, College of Science, Princess Nourah bint Abdulrahman University, P.O. Box 84428, Riyadh 11671, Saudi Arabia, e-mail: maalnoussier@pnu.edu.sa

1 Introduction

Hydrogen gas is essential for achieving a decarbonized energy system and meeting emission reduction goals, such as those in the Paris Agreement. Producing green hydrogen *via* water splitting powered by renewable energy, particularly solar power, is a promising approach [1,2]. Solar energy, with over 520 GW of global capacity as of 2018, is cost-effective and widely deployed, making it ideal for hydrogen production [3,4]. Hydrogen serves as a key energy carrier in transportation, heating, industrial processes, and power generation. Regions with abundant solar resources, like the Middle East and North Africa, are well-positioned for green hydrogen production. On a global scale, green hydrogen is expected to be traded within emission-neutral systems, requiring advancements in technology, infrastructure, and comprehensive evaluations of production and distribution to support effective policies [5]. Hydrogen's potential applications include fueling non-polluting vehicles, heating, and aviation. As such, it is anticipated to become a major component of a sustainable energy future, alongside solar energy.

Photocatalysis is a valuable process that uses light to drive reactions through electron transfer facilitated by semiconductor materials [6,7]. To improve hydrogen production rates, photocatalytic materials must possess a high surface area and abundant active sites. Structures such as nanorods, nanowires, and sheet-like materials show significant potential for enhancing hydrogen generation.

Additionally, composite materials, which integrate diverse optical and surface characteristics, offer further advantages by optimizing performance and efficiency [8,9].

In recent years, metal oxides and sulfides that respond to visible light have gained attention for their hydrogen generation potential. Notable examples include WO_3 (2.7 eV), Bi_2O_3 (2.6–2.8 eV), $SrNbO_3$ (2.3 eV), and CdS (2.4 eV). Bismuth-based semiconductor Bi_2O_3, in particular, has emerged as a viable alternative due to its low toxicity. Bi_2O_3 typically exists in two main polymorphs: monoclinic α phase (~2.8 eV) and tetragonal β phase (~2.6 eV). To enhance the photocatalytic performance of Bi_2O_3, one effective strategy is to employ heterostructures. These heterostructures, created by combining different materials, can modify the electronic band structure at their interfaces [10]. Bismuth oxide chloride (BiOCl) is a particularly suitable material for this purpose due to its compatibility with Bi_2O_3, as both share the same element, bismuth, and BiOCl has a similar band gap [11,12]. The layered structure of BiOCl helps to reduce the distance for photoelectron transmission, thereby improving the separation of photogenerated electron–hole pairs. This enhances the photocatalytic efficiency. Combining a narrow band gap with a unique nanostructure is an effective approach to achieving both visible light responsiveness and a high quantum yield.

Poly *m*-toluidine (PMT) is another promising material due to its optical properties, which are similar to those of polyaniline (PANI) but with additional benefits. These properties, including strong light absorption and high stability, make PMT suitable as an electrode material for water-splitting reactions and hydrogen production [13]. When exposed to light, these materials absorb photons, which leads to surface activation and the generation of electron–hole pairs. The generated electrons then interact with water molecules in a complex process that produces free radicals, ultimately resulting in the production of hydrogen gas. Furthermore, poly-1*H* pyrrole (P1HP) exhibits excellent semiconductor properties and outstanding morphological characteristics. It is synthesized with minimal particle content, making it an effective seeding material and a highly efficient photocatalytic layer.

Previous studies on H_2 gas generation have encountered various technical challenges, including the need for external electrolytes, such as harsh acids or bases. Other research has relied on bulk materials without adequately addressing morphological features, while some studies have employed highly complex techniques for hydrogen generation.

In this work, a novel BiOCl/PMT/P1HP photocathode was synthesized using a one-pot technique to create the BiOCl/PMT composite on the surface of a P1HP thin film. Various analyses confirmed the chemical characteristics and morphological properties of this composite. The photocathode was then integrated into a three-electrode cell to generate H_2 gas by splitting sewage water, introducing a new source of hydrogen. The reaction was conducted under different optical conditions, including white light and photon energies ranging from 1.7 to 3.6 eV. The sensitivity of the photocathode was assessed using chopped light, and the amount of H_2 produced was calculated using Faraday's law.

2 Materials and methods

2.1 Materials

Bismuth nitrate ($Bi(NO_3)_3$ 99.9%, Pio-Chem Co., Egypt), HCl (36%, Merck, Germany), ethanol (C_2H_5OH, 99.9%, Merck, Germany), *m*-toluidine (99.9%, Merck, Germany), $(NH_4)_2S_2O_8$ (99.9%, Pio-Chem Co., Egypt), and sanitation water (third treated, water company, Beni Suef City, Egypt) were used in this study.

2.2 Characterization techniques

The characterization of nanomaterials was performed using various advanced techniques. Surface morphology and three-dimensional features were analyzed using a scanning electron microscope (SEM, Zeiss, Germany), while the internal structure and two-dimensional characteristics were examined using a transmission electron microscope (TEM, JEOL, Japan). Elemental oxidation states were determined using an X-ray photoelectron spectroscopy (XPS) device (Kratos, UK), and crystalline properties were studied *via* X-ray diffraction (XRD) analysis (Xpert, Netherlands) within a 2θ range of 10° to 62°. Functional group identification and optical properties were assessed using a Fourier Transform Infrared (FTIR) spectrometer (Bruker) across a spectral range of 750–3,500 cm^{-1}, complemented by a PerkinElmer instrument from the USA for further analysis. This combination of techniques provided comprehensive insights into the nanomaterial's surface, structural, elemental, and optical characteristics.

2.3 Fabrication of BiOCl/PMT/P1HP photocathode through the oxidation polymerization

The BiOCl/PMT/P1HP photocathode is synthesized through an oxidative polymerization reaction of *m*-toluidine in the presence of $Bi(NO_3)_3$, using $(NH_4)_2S_2O_8$ as the oxidizing agent. In this process, the monomer and $Bi(NO_3)_3$ are dissolved in HCl, maintaining a molar ratio of 1:1:10. Meanwhile, $(NH_4)_2S_2O_8$ is dissolved in water at a concentration of 0.1 M. Once both the monomer and oxidant solutions are fully dissolved, the oxidant is added to the monomer solution, initiating the polymerization reaction. This reaction results in the formation of Bi_2O_3 intercalated within the PMT network, along with BiOCl.

The resulting BiOCl/PMT/P1HP nanocomposite thin film undergoes treatment and drying processes to prepare it for further analysis and applications.

The fabrication of the P1HP seeding layer follows a previously established method [14], which involves the oxidation of pyrrole using $(NH_4)_2S_2O_8$ in an acidic medium. This method, detailed in our earlier publications, provides a foundation for the creation of the seeding layer, ensuring consistency and reliability in the overall fabrication process.

2.4 Photoelectrochemically H_2 generation using the BiOCl/PMT/P1HP photocathode

The photoelectrochemical generation of hydrogen is conducted *via* the splitting of sanitation water using a specially fabricated BiOCl/PMT/P1HP photocathode. In this setup, the photocathode serves as the working electrode within the cell. Sanitation water is chosen as the electrolyte due to its low cost with its constituents (Table 1), and its conversion into a renewable energy source represents a dual benefit: not only does it generate energy in the form of H_2 gas, but it also transforms harmful wastewater into something useful.

The experimental setup includes a three-electrode cell configuration. Alongside the working electrode, a calomel electrode is used to estimate the potential inside the cell, while another calomel electrode helps provide the current without inducing any additional chemical reactions. The efficiency of H_2 gas evolution through the photoelectrochemical reaction is assessed by measuring the current density under illumination (J_{ph}), which serves as an excellent indicator. This value is compared to the dark current density (J_o), allowing for the determination of the enhancement brought about by the light.

A vacuum halide metal lamp, which can produce white light, serves as the light source. To control the wavelengths of light that reach the photocathode, a series of monochromatic filters are employed. These filters allow only specific wavelengths of light to pass through, thus enabling precise control over the photoelectrochemical reactions.

The generation of H_2 gas is quantified using the photoinduced current density (J_{ph}). By evaluating the J_{ph} values at different wavelengths and comparing them to J_o, the amount of H_2 produced can be estimated (Figure 1). This estimation takes into account the time intervals during which H_2 gas is produced. The number of moles of H_2 generated is calculated using an established equation (Eq. (1)) [15], which incorporates the J_{ph} value and the duration of gas production

$$H_2 \text{ mole} = \int_0^t J_{ph} \cdot dt/F. \tag{1}$$

Table 1: Concentration of ions in sanitation water (μg/L) [16]

Material or element	Concentration (μg/L)
F^-	1,000
Hg^{2+}	5
Ni^{3+}	100
Phenols	150
Mn^{2+}	1,000
NH_3	5,000
Ba^{3+}	2,000
Al^{3+}	3,000
Cd^{3+}	50
Cr^{3+}	1,000
As^{3+}	50
Pb^{2+}	500
Co^{2+}	2,000
Cu^{2+}	15,000
Zn^{2+}	5,000
Fe^{3+}	1,500
Pesticides	200
Ag^+	100
Industrial washing	500
CN^{-1}	100
Other cations	100
Coli groups	4,000/0.1 cm^3

3 Results and discussion

3.1 BiOCl/PMT nanocomposite physiochemical analyses

Understanding the crystalline size and properties of the synthesized BiOCl/PMT nanocomposite is essential to grasp its optical applications. PMT, in its pristine state, exhibits non-crystalline behavior. However, this characteristic significantly improves upon forming the composite, as shown in Figure 2(a). The synthesized polymer within the

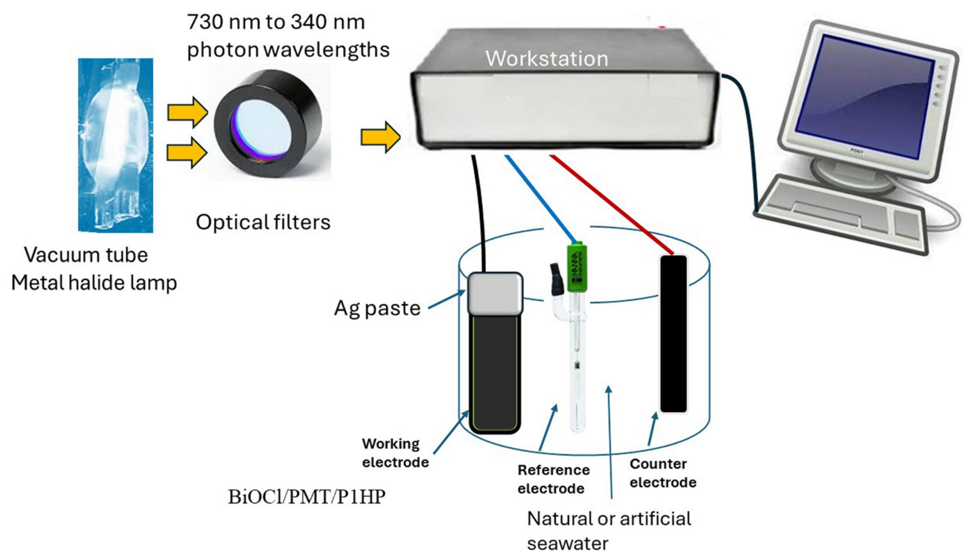

Figure 1: Procedures for the applications of BiOCl/PMT/P1HP photocathode inside three-electrode for H_2 gas generation.

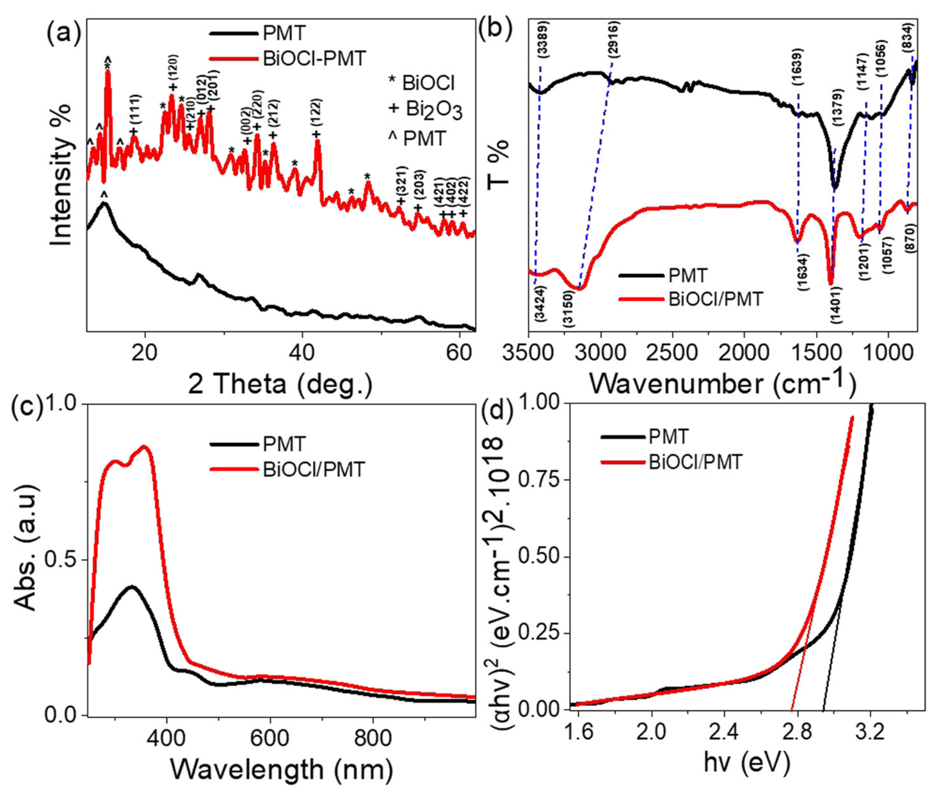

Figure 2: Physicochemical analyses of the BiOCl/PMT nanocomposite: (a) XRD analysis, (b) FTIR analysis, and (c) and (d) optical analyses, including absorbance and the corresponding evaluated bandgap.

composite shows substantial crystallinity, indicated by five distinct crystalline peaks within the range of 11–19.6°, which enhance its photon absorption capability.

Moreover, the nanocomposite shows the interaction with BiOCl materials, indicated by a sharp peak at 15.3° and seven additional low-intensity peaks at 48.5°, 46.2°, 38.9°, 35.3°, 30.9°, 24.5°, and 22.4°, JCPDS (06-0249) [17]. These peaks further enhance the composite's overall feature for light absorbance, as they contribute to trapping photons.

The incorporated inorganic Bi_2O_3 component with a few percent displays some crystallinity, evidenced by 14 distinct peaks. Among these, seven peaks demonstrate high crystallinity intensities at 42.0°, 36.3°, 34.3°, 32.6°, 28.1°, 27.0°, and 23.3°, corresponding to the growth directions (122), (212), (220), (002), (201), (012), and (120), respectively. Additionally, there are seven more peaks with lower intensity but still indicative of the nanocomposite's crystallinity. These peaks are located at 60.4°, 59.1°, 58.0°, 54.7°, 52.4°, 25.6°, and 18.7°, corresponding to growth directions (422), (402), (421), (203), (321), (002), and (111), respectively. This crystallinity feature is confirmed by the JCBDS standard 76-1730 [10,18].

The very small crystalline size of about 39 nm, estimated using the Scherrer equation (Eq. (2)) [19] based on the highly crystalline peak at 42.0°, also contributes to this enhanced light absorption capability. So, the combination of BiOCl and Bi_2O_3 with PMT improves crystallinity in the composite form, resulting in a material with highly light-absorbing properties

$$D = 0.9\lambda/\beta \;\; \cos\theta. \quad (2)$$

In addition to analyzing the crystalline structure of the synthesized BiOCl/PMT nanocomposite, the functional groups within the composite were identified using FTIR analysis, as illustrated in Figure 2(b). This analysis revealed the presence of all anticipated functional groups at their respective wavenumber positions. Table 2 provides a summary of these groups and their positions. The FTIR analysis indicated that the polymer's functional groups are present in the composite, with shifts reflecting the integration of Bi_2O_3 materials.

The composite exhibits a red-shift in most of these groups, which can be attributed to the incorporation of Bi_2O_3 or BiOCl within the structure. Additionally, there is a significant change in the intensity of the band at 870 cm^{-1}, corresponding to the Bi–O bond. This shift and change in intensity highlight the insertion of the inorganic components into a polymer matrix [20], supporting the successful formation of the Bi_2O_3–PMT nanocomposite and providing insights into its structure and properties.

Table 2: Estimated band positions of the BiOCl/PMT nanocomposite relative to the PMT polymer through the estimated FTIR analyses

Group and its value (cm^{-1})		Function group
BiOCl/PMT	**PMT**	
870	834	C–H out of plan
1,201 and 1,057	1,147 and 1,056	C–H group
1,401	1,379	C–N
1,634	1,639	C–C
3,424	3,389	N–H

The behavior of the BiOCl/PMT nanocomposite in terms of optical absorption and the subsequent generation of hot electrons, which act as attaching electrons during H_2 gas generation, is evaluated through the optical absorption spectra shown in Figure 2(c). The formation of the composite leads to a significant enhancement in the π–π* transition and the production of hot electrons. This improvement is due to the synergistic optical effect of combining Bi_2O_3 and PMT, which together maximize the generation of hot electrons essential for H_2 production during the solution reaction.

The composite exhibits maximum absorption in the UV and the initial visible (Vis) region up to 430 nm, with the formation of a broad absorption band extending to 800 nm, reaching into the IR region. This broad absorption indicates a substantial enhancement in the optical behavior of PMT following the formation of the composite. These optical properties are further quantified by evaluating the bandgap value using Tauc equations (Eqs. (3) and (4)) [21]. The bandgap for the nanocomposite is estimated to be 2.75 eV, reflecting its improved optical characteristics (Figure 2(d))

$$\alpha = \left(\frac{2,303}{t}\right)A, \quad (3)$$

$$\alpha h\nu = A(h\nu - E_g)^{1/2}. \quad (4)$$

The structure of the BiOCl/PMT nanocomposite, along with the oxidation states of its elements, has been analyzed using XPS, as shown in Figure 3(a). The XPS survey reveals the presence of all the expected elements within the composite, including chlorine, which is detected at around 200 eV. The elements associated with the PMT polymer are also identified, with the carbon element's 1s orbital appearing at 285.3 eV and the nitrogen element's 1s orbital observed at 400 eV. The XPS for bismuth (Bi) elements indicates the duplicated peaks at 160.3 and 165.8 eV. These shifted peaks are depicted in Figure 3(b).

The presence of traces within Bi_2O_3 is evaluated through the characteristic peaks corresponding to the Bi $4f_{7/2}$ and Bi $4f_{5/2}$ orbitals, which are located at 159.6 and 165.1 eV, respectively [11,12]. These peaks are critical indicators of the presence of Bi_2O_3 in the composite.

Further analysis of the chlorine (Cl) element and the oxygen (O) 1s spectrum, which appears at 532 eV, provides additional evidence supporting the formation of both Bi_2O_3 and BiOCl within the PMT matrix. The combination of these

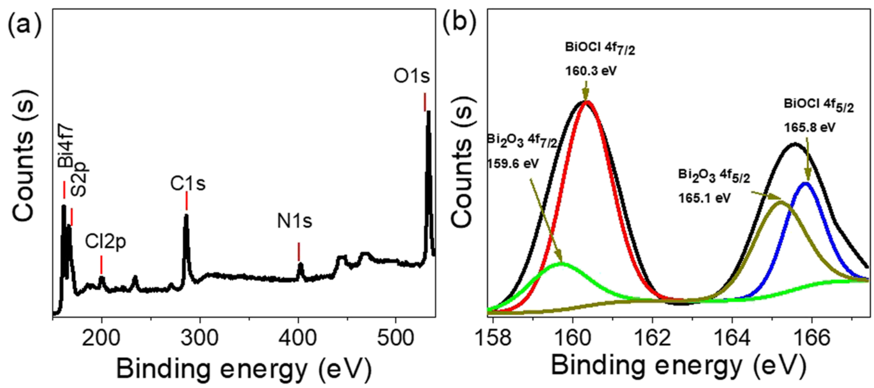

Figure 3: XPS chemical analyses of the BiOCl/PMT nanocomposite: (a) survey and (b) Bi element.

spectral findings underscores the successful integration of Bi_2O_3 and BiOCl materials into the PMT nanocomposite, demonstrating the complex structure and the effective oxidation states of the involved elements.

The morphological structure of the fabricated BiOCl/PMT nanocomposite, compared to that of pure PMT, is analyzed and presented in Figure 4. The SEM analysis of the composite (Figure 4(a)) reveals the formation of a

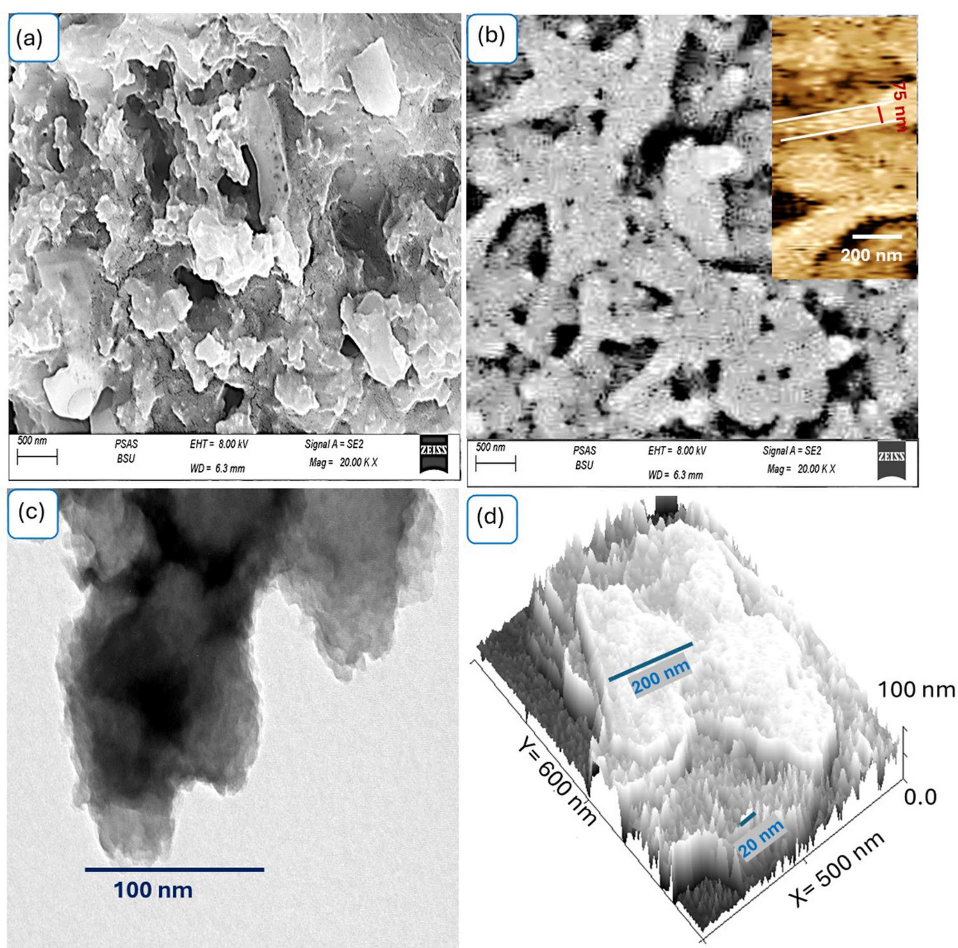

Figure 4: SEM morphological analyses of the synthesized nanomaterials: (a) BiOCl/PMT nanocomposite and (b) PMT, whereas (c) TEM and (d) theoretical modeling for BiOCl/PMT nanocomposite.

highly porous, non-uniform structure. This morphology arises from the aggregation of small particles, each with an average size of approximately 50 nm, which coalesce to form larger particles around 500 nm in size. This porous structure is advantageous as it allows photons to pass through and become trapped within, enabling multiple scattering events. These events result in the generation and collection of a large number of hot electrons on the surface of the structure, which can then participate in further reactions with nearby solutions [22–24]. In Figure 4(c), the composite's compact nature is further illustrated. The image shows the integration of inorganic materials, which appear as dark regions, within the PMT matrix, which is displayed as a lighter shell. This contrast highlights the effective incorporation of Bi_2O_3 into the PMT structure.

Figure 4(d) provides a more detailed view of the composite's structure. It shows that the polymer forms a highly porous outer layer, with small particles around 20 nm in size aggregating into larger structures approximately 300 nm thick. The central particles within the composite are densely packed, forming larger clusters with diameters of about 200 nm.

These structural features of the BiOCl/PMT nanocomposite are significantly different from those of pure PMT, as depicted in Figure 4(b). The PMT is shown to form a small, complex network with a longitudinal shape with an average diameter of 75 nm. In addition to their spherical shape, these particles exhibit some porosity, which suggests that the PMT alone can form structures with different characteristics when compared to the composite.

Overall, the SEM analysis reveals that the BiOCl/PMT nanocomposite has a complex, porous structure that is distinct from the simpler, spherical morphology of pure PMT. This intricate structure is crucial for the composite's enhanced optical properties, as it facilitates efficient photon trapping and electron generation.

3.2 BiOCl/PMT/P1HP photocathode green H_2 generation electrochemistry

The generation of green hydrogen in this study is carried out through electrochemical splitting of sewage water within a three-electrode cell. The reduction reactions necessary for this process occur on the surface of a specially fabricated photocathode. This photocathode, made of BiOCl/PMT/P1HP, plays a crucial role in generating hot electrons. These hot electrons act as the key initiators for producing hydroxyl ($OH^{\cdot}$) radicals, which subsequently drive the splitting reaction in the surrounding solution. The amount of hydrogen gas (H_2) produced is directly related to the generation of hot electrons, which can be estimated through the measurement of the J_{ph}. The value of J_{ph} provides insight into the efficiency of electron generation, and therefore, the amount of hydrogen gas that is produced.

A notable advantage of this process is the use of sewage water as the source for hydrogen production. By utilizing a contaminated water source, the overall economic feasibility of hydrogen generation is significantly improved. This makes the system an attractive solution for addressing energy shortages, as it transforms waste into a renewable energy source. The use of a vacuum tube metal halide for illumination provides white light that enhances the photocathode's performance. Under illumination, the measured J_{ph} value is −0.046 mA/cm^2, which decreases to −0.032 mA/cm^2 when the light is turned off, as illustrated in Figure 5(a). The difference between these values corresponds to the photocurrent (0.012 mA/cm^2), demonstrating the photocathode's excellent photoelectrochemical behavior under illumination. This result highlights the efficient transfer of hot electrons from the PMT layer to the Bi_2O_3 layer, with Bi_2O_3 serving as the electron initiator for reactions in the adjacent sanitation solution. Meanwhile, the holes move in the opposite direction [25], accumulating on the PMT surface.

The photocathode's stability plays a vital role in its overall performance. Its durability ensures consistent behavior, as evidenced by the current density fluctuations observed under conditions of alternating illumination and darkness. These variations in current density, which can be seen in Figure 5(b), demonstrate the reproducibility and sensitivity of the fabricated photocathode. The consistent increase and decrease in current densities, depending on whether the photocathode is illuminated or in darkness, indicate a high degree of stability and reliability. This research holds significant promise, particularly in terms of using contaminated water as a resource for generating renewable energy. The use of sewage water not only reduces costs but also presents a sustainable solution to the world's energy challenges [26]. The materials used in the photocathode, particularly BiOCl and PMT, show strong potential for long-term application due to their stability and efficient electron transfer properties. As the photocurrent values directly reflect the amount of hydrogen produced, this method of hydrogen generation could become a pivotal technology in the renewable energy sector, especially in addressing global energy shortages while managing environmental waste effectively.

The behavior of the photocathode during sewage water splitting can be influenced by varying the photon energies,

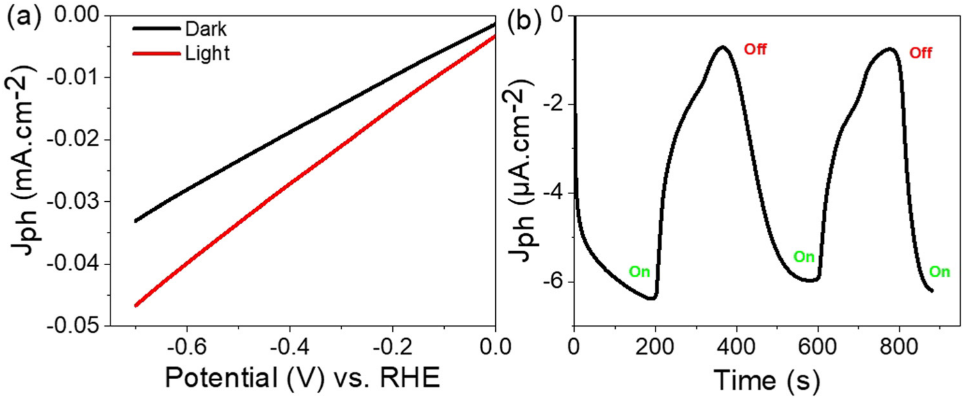

Figure 5: (a) Electrochemical performance of the fabricated photocathode under illumination and (b) the sequential variation in the generated current corresponding to the chopped light exposure on the BiOCl/PMT/P1HP photocathode.

which can be adjusted between 3.6 and 1.7 eV using filters that control the wavelengths of the photons. As the photon energies increase, the energy transferred to the photocathode also rises, leading to a significant increase in the generation of electrons on the surface of the BiOCl/PMT/P1HP photocathode. These generated electrons are crucial for producing hot electrons with varying kinetic energies. This variation is reflected in the linear sweep voltammetry curves, which show changes in the J_{ph}. The J_{ph} values shift from −0.045 mA/cm² at 3.4 eV to approximately −0.042 mA/cm² at 1.7 eV under an applied bias voltage of −0.7 V, as illustrated in Figure 6(a). Notably, there is optimization at photon energies of 3.6 and 2.8 eV, which are higher than the evaluated bandgap of 2.75 eV, indicating that these photons possess sufficient energy to provide additional kinetic energy for the reaction. The summary of these J_{ph} values is presented in Figure 6(b). This behavior underscores the high sensitivity of the fabricated photocathode, which is based on the excellent photocatalytic properties of the semiconductor materials BiOCl and PMT.

The sensitivity of the fabricated BiOCl/PMT/P1HP photocathode is assessed by measuring the amount of H_2 gas evolved, as shown in Figure 7(a). The production rate of H_2 gas is estimated to be 15 µmol/h for a 10 cm² area. These values are closely tied to the sequential transfer of photogenerated charges, which involves the movement of generated electrons and holes in opposite directions under the small bandgap of 2.75 eV. Hot electrons accumulate on the BiOCl material and then migrate into the solution to drive the water-splitting reaction, leading to H_2 gas generation. Simultaneously, the holes move in the opposite direction until they reach the PMT material, creating polarization during this process. This charge movement is facilitated by the close alignment of the conduction and valence levels of PMT and BiOCl, enhancing the efficiency of charge transfer, as depicted in Figure 7(b). The flow of these

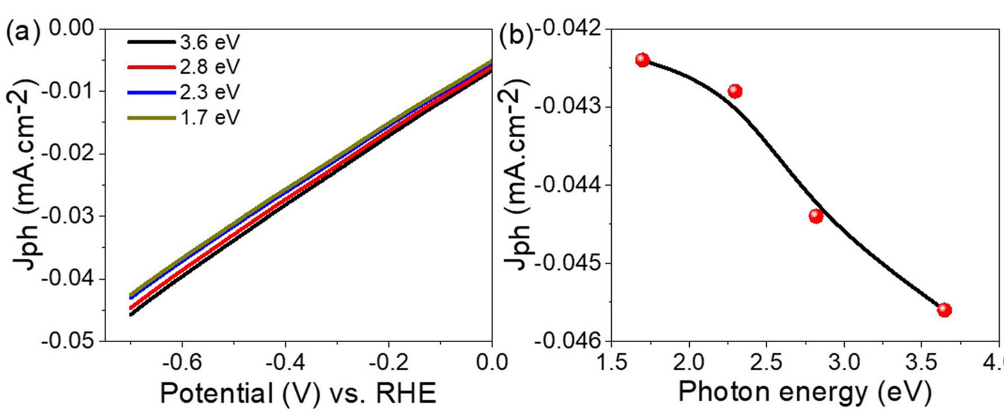

Figure 6: (a) Electrochemical performance of the fabricated BiOCl/PMT/P1HP photocathode under illumination with different photon energies and (b) the variation in the produced current corresponding to these changes in photon energy.

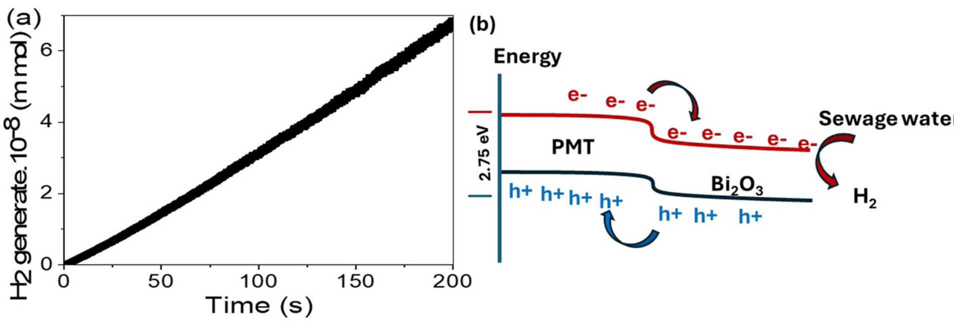

Figure 7: (a) Electrochemical performance under illumination for H_2 moles produced and (b) the sequential charge transfer through the constituents of the BiOCl/PMT/P1HP photocathode.

generated electrons into the neighboring solution results in the formation of OH radicals, which further support the water-splitting reaction [27].

Utilizing sewage water in this process presents an excellent option for generating H_2 gas from waste and contaminated water, making this study highly promising. When compared to other materials in the literature, such as Cr_2S_3-Cr_2O_3/poly-2-aminobenzene-1-thiol [28] or graphene oxide/polypyrrole [29], which achieves about 0.01 mA/cm² with limited H_2 production, this photocathode demonstrates superior performance.

4 Conclusions

A novel BiOCl/PMT/P1HP photocathode has been created for generating H_2 gas from sewage water. This BiOCl/PMT composite features a crystalline size of 39 nm, a bandgap of 2.75 eV, and a porous polymer structure with 20 nm pores that aggregate into larger structures around 300 nm thick.

When used as the working electrode in a three-electrode cell, the BiOCl/PMT/P1HP photocathode achieves a hydrogen production rate of 15 µmol/h over a 10 cm² area. The J_{ph} measures −0.046 mA/cm² under illumination, decreasing to −0.032 mA/cm² when the light is turned off, resulting in a photocurrent of 0.012 mA/cm². This reflects the photocathode's highly efficient photoelectrochemical behavior. The performance of this photocathode in splitting sewage water can be finely tuned by adjusting the photon energies between 3.6 and 1.7 eV using filters to control the photon wavelengths. This variation is observed in the linear sweep voltammetry curves, where J_{ph} values shift from −0.045 mA/cm² at 3.4 eV to approximately −0.042 mA/cm² at 1.7 eV under an applied bias voltage of −0.7 V. The promising efficiency of this photocathode, coupled with its cost-effectiveness, positions the BiOCl/PMT/P1HP photocathode as a compelling choice for green chemistry applications and industrial-scale hydrogen production.

Acknowledgments: Princess Nourah bint Abdulrahman University Researchers Supporting Project number (PNURSP2024R186), Princess Nourah bint Abdulrahman University, Riyadh, Saudi Arabia.

Funding information: This work was funded by Princess Nourah bint Abdulrahman University Researchers Supporting Project number (PNURSP2024R186), Princess Nourah bint Abdulrahman University, Riyadh, Saudi Arabia.

Author contributions: All authors have accepted responsibility for the entire content of this manuscript and approved its submission.

Conflict of interest: The authors state no conflict of interest.

Data availability statement: All data generated or analyzed during this study are included in this published article.

References

[1] Kountouris I, Bramstoft R, Madsen T, Gea-Bermúdez J, Münster M, Keles D. A unified European hydrogen infrastructure planning to support the rapid scale-up of hydrogen production. Nat Commun. 2024;15(1):1–13. doi: 10.1038/s41467-024-49867-w.

[2] de Kleijne K, Huijbregts MAJ, Knobloch F, van Zelm R, Hilbers JP, de Coninck H, et al. Worldwide greenhouse gas emissions of green hydrogen production and transport. Nat Energy. 2024;2024:1–14. doi: 10.1038/s41560-024-01563-1.

[3] Zhao W, Luo L, Cong M, Liu X, Zhang Z, Bahri M, et al. Nanoscale covalent organic frameworks for enhanced photocatalytic hydrogen production. Nat Commun. 2024;15(1):1–11. doi: 10.1038/s41467-024-50839-3.

[4] Zhang Y, Wan J, Zhang C, Cao X. MoS2 and Fe2O3 Co-modify g-C3N4 to improve the performance of photocatalytic hydrogen

production. Sci Rep. 2022;12(1):1–12. doi: 10.1038/s41598-022-07126-2.
[5] Giuntoli F, Menegon L, Siron G, Cognigni F, Leroux H, Compagnoni R, et al. Methane-hydrogen-rich fluid migration may trigger seismic failure in subduction zones at forearc depths. Nat Commun. 2024;15(1):1–16. doi: 10.1038/s41467-023-44641-w.
[6] Xie H, Zhao Z, Liu T, Wu Y, Lan C, Jiang W, et al. A membrane-based seawater electrolyser for hydrogen generation. Nature. 2022;612(7941):673–8. doi: 10.1038/s41586-022-05379-5.
[7] Jovičević-Klug M, Souza Filho IR, Springer H, Adam C, Raabe D. Green steel from red mud through climate-neutral hydrogen plasma reduction. Nature. 2024;625(7996):703–9. doi: 10.1038/s41586-023-06901-z.
[8] Li T, Wang B, Cao Y, Liu Z, Wang S, Zhang Q, et al. Energy-saving hydrogen production by seawater electrolysis coupling tip-enhanced electric field promoted electrocatalytic sulfion oxidation. Nat Commun. 2024;15(1):1–12. doi: 10.1038/s41467-024-49931-5.
[9] Tsao CW, Narra S, Kao JC, Lin YC, Chen CY, Chin YC, et al. Dual-plasmonic Au@Cu7S4 Yolk@shell nanocrystals for photocatalytic hydrogen production across visible to near infrared spectral region. Nat Commun. 2024;15(1):1–13. doi: 10.1038/s41467-023-44664-3.
[10] Jabeen Fatima MJ, Niveditha CV, Sindhu S. α-Bi2O3 photoanode in DSSC and study of the electrode–electrolyte interface. RSC Adv. 2015;5:78299–305. doi: 10.1039/C5RA12760B.
[11] Zhang M, Duo F, Lan J, Zhou J, Chu L, Wang C, et al. In situ synthesis of a Bi2O3 quantum dot decorated BiOCl heterojunction with superior photocatalytic capability for organic dye and antibiotic removal. RSC Adv. 2023;13:5674–86. doi: 10.1039/D2RA07726D.
[12] Wu K, Qin Z, Zhang X, Guo R, Ren X, Pu X. Z-scheme BiOCl/Bi–Bi2O3 heterojunction with oxygen vacancy for excellent degradation performance of antibiotics and dyes. J Mater Sci. 2020;55:4017–29. doi: 10.1007/S10853-019-04300-2.
[13] Kedir CN, Salinas-Torres D, Quintero-Jaime AF, Benyoucef A, Morallon E. Hydrogels obtained from aniline and piperazine: Synthesis, characterization and their application in hybrid supercapacitors. J Mol Struct. 2022;1248:131445. doi: 10.1016/J.MOLSTRUC.2021.131445.
[14] Alkallas FH, Elsayed AM, Trabelsi ABG, Rabia M. Porous-spherical MnO2-Mn(OH)2/polypyrrole nanocomposite thin film photodetector in a wide optical range from UV to IR. Opt Quantum Electron. 2023;55:1–15. doi: 10.1007/S11082-023-05260-3/METRICS.
[15] Rabia M, Elsayed AM, Alnuwaiser MA. Mn (IV) oxide/Mn (IV) sulfide/poly-2-amino-1-mercaptobenzene for green hydrogen generation. Surf Innov. 2023;12(5–6):282–91. doi: 10.1680/JSUIN.23.00031.
[16] Hadia NMA, Abdelazeez AAA, Alzaid M, Shaban M, Mohamed SH, Hoex B, et al. Converting sewage water into H2 fuel gas using Cu/CuO nanoporous photocatalytic electrodes. Materials. 2022;15:1489. doi: 10.3390/MA15041489.
[17] Li L, Zhang M, Zhao Z, Sun B, Zhang X. Visible/near-IR-light-driven TNFePc/BiOCl organic-inorganic heterostructures with enhanced photocatalytic activity. Dalton Trans. 2016;45:9497–505. doi: 10.1039/c6dt01091a.
[18] Jiang M, Ding Y, Zhang H, Ren J, Li J, Wan C, et al. A novel ultrathin single-crystalline Bi2O3 nanosheet wrapped by reduced graphene oxide with improved electron transfer for Li storage. J Solid State Electrochem. 2020;24:2487–97. doi: 10.1007/S10008-020-04788-8/FIGURES/10.
[19] Ahmed AM, Rabia M, Shaban M. The structure and photoelectrochemical activity of Cr-doped PbS thin films grown by chemical bath deposition. RSC Adv. 2020;10:14458–70. doi: 10.1039/c9ra11042a.
[20] Ashwini IS, Pattar J, Sreekanth R, Nagaraja M, Manohara SR, Anjaneyulu P. Synthesis, electrical, and dielectric properties of novel polyaniline/strontium di-nitrate composites. Polym Compos. 2021;42:5125–33. doi: 10.1002/PC.26210.
[21] Aziz SB, Nofal MM, Ghareeb HO, Dannoun EMA, Hussen SA, Hadi JM, et al. Characteristics of poly(vinyl alcohol) (PVA) based composites integrated with green synthesized Al^{3+} -metal complex: Structural, optical, and localized density of state analysis. Polymers. 2021;13:1316. doi: 10.3390/POLYM13081316.
[22] Elsayed AM, Shaban M, Aly AH, Ahmed AM, Rabia M. Preparation and characterization of a high-efficiency photoelectric detector composed of hexagonal Al2O3/TiO2/TiN/Au nanoporous array. Mater Sci Semicond Process. 2022;139:106348. doi: 10.1016/J.MSSP.2021.106348.
[23] An X, Kays JC, Lightcap IV, Ouyang T, Dennis AM, Reinhard BM. Wavelength-dependent bifunctional plasmonic photocatalysis in Au/chalcopyrite hybrid nanostructures. ACS Nano. 2022;16:6813–24. doi: 10.1021/ACSNANO.2C01706/SUPPL_FILE/NN2C01706_SI_001.PDF.
[24] Sharma U, Karazhanov S, Jose R, Das S. Plasmonic hot-electron assisted phase transformation in 2D-MoS2 for the hydrogen evolution reaction: current status and future prospects. J Mater Chem A. 2022;10(16):8626–55. doi: 10.1039/D1TA10918A.
[25] Zhu W, Yang L, Liu F, Si Z, Huo M, Li Z, et al. Metal Ni nanoparticles in-situ anchored on CdS nanowires as effective cocatalyst for boosting the photocatalytic H2 production and degradation activity. J Alloy Compd. 2024;973:172747. doi: 10.1016/j.jallcom.2023.172747.
[26] Aldosari E, Rabia M, Abdelazeez AA. Rod-shaped Mo(VI) Trichalcogenide – Mo(VI) oxide decorated on poly(1-H pyrrole) as a promising nanocomposite photoelectrode for green hydrogen generation from sewage water with high efficiency. Green Process Synth. 2024;13:20230243.
[27] Jia C, Guo J, Hu Y, Li T, Zhou T, Liang X, et al. Synthesis of multifunctional magnetic mesoporous Fe3O4@MSN@PPy-HA nanospheres for PH-responsive drug release and photothermal in tumor therapy. Colloids Surf A: Physicochem Eng Asp. 2023;675:132077. doi: 10.1016/J.COLSURFA.2023.132077.
[28] Rabia M, Elsayed AM, Alnuwaiser MA. Cr2S3-Cr2O3/poly-2-aminobenzene-1-thiol as a highly photocatalytic material for green hydrogen generation from sewage water. Micromachines. 2023;14:1567. doi: 10.3390/MI14081567.
[29] Hamid MMA, Alruqi M, Elsayed AM, Atta MM, Hanafi HA, Rabia M. Testing the photo-electrocatalytic hydrogen production of polypyrrole quantum dot by combining with graphene oxide sheets on glass slide. J Mater Sci: Mater Electron. 2023;34:1–11. doi: 10.1007/S10854-023-10229-9/METRICS.